MOX-Report No. 42/2020

A spatio-temporal model with multi-city mobility for COVID-19 epidemic

Miglio, E.; Parolini, N.; Quarteroni, A.; Verani, M.; Zonca, S.

MOX, Dipartimento di Matematica
Politecnico di Milano, Via Bonardi 9 - 20133 Milano (Italy)

mox-dmat@polimi.it http://mox.polimi.it

A spatio-temporal model with multi-city mobility for COVID-19 epidemic

Edie Miglio[1], Nicola Parolini[1], Alfio Quarteroni[1,2], Marco Verani[1], and Stefano Zonca[1]

[1]MOX, Department of Mathematics, Politecnico di Milano, Italy
[2]Institute of Mathematics, Ecole Polytechnique Fédérale de Lausanne (EPFL), Switzerland (Professor Emeritus)

October 28, 2020

Abstract

The COVID-19 epidemic is the last of a long list of pandemics that have affected human kind in the last century. The virus spread very quickly all over the world due to the structure of modern society where mobility is very high. In this paper we aim at a critical study of a multi-city model consisting of 8 compartments for describing the spreading of a disease. A convenient parameter calibration is implemented with the aim of reproducing the past history of the epidemic and of exploring its predicting capabilities.

1 Introduction

The COVID-19 epidemic is a tremendous threat to global health. Since the outbreak in early December 2019 in China, more than 473.000 people have died from COVID-19, while the total number of confirmed patients having the disease is 9.158.912 (up to 23 June 2020, [1]). The real number of people infected is unknown, but probably much higher.

In this scenario, predicting the trend of the epidemic is of paramount importance to mitigate the pressure on the health systems and activate control strategies (e.g. quarantines, lockdowns, and suspension of travel) aiming at containing the disease and delaying the spread.

As these predictions have vital consequences on the different actions taken from governments to limit and control the COVID-19 epidemic, the recent period has seen an astonishing production of numerous epidemiological mathematical models. However, estimates and scenarios emerging from modeling highly depend on different factors, ranging from epidemiological assumptions to, perhaps most importantly, the completeness and the quality of the data to which models are calibrated. Since the beginning of the COVID-19 emergency, the quality of data on infections, deaths, tests, and other factors have been spoiled by underdetection or inconsistent detection of cases, reporting delays, and poor documentation. This inconvenient has seriously compromised the intrinsic predictive capability of any mathematical model.

Building upon the celebrated SIR model proposed in 1927 by Kermack and McKendrick ([12]), several generalizations have been formulated over the years by enriching the number of compartments (SEIR, SIS, SEIRD, SIRS, S(E)IQR, MSEIR ...), see, e.g., [11, 6, 15] for an overview. Over-

all, these models have been abundantly applied to locally analyze COVID-19 outbreak dynamics in various countries (see, e.g., [14, 13]).

However, the peculiar epidemiological traits of the COVID-19 ask for more complex models able to accurately portray the dynamic characteristics of the ongoing epidemic. We refer, for instance, to [10] and the references therein. In particular, in [10] a new model, named SIDARTHE, discriminates between detected and undetected cases of infection, either asymptomatic or symptomatic, and also between non-life-threatening cases (minor and moderate infection) and potentially life-threatening cases (major and extreme) that require Intensive Care Unit (ICU) admission. These last two compartments are of paramount importance in designing realistic scenarios that incorporate the pressure of the epidemic on the national health systems. On the other hand, human mobility has played a far-reaching role in the diffusion of the COVID-19 contagions. This requires to incorporate into the mathematical model the spatial nature of the progress of the wave of infections. In this respect several different approaches have been proposed in the literature, see, e.g., the book [7] and the references therein, ranging from the use of network based model [4, 8], to systems of ODEs on network [3, 2], to non-local PDEs [16]. Among the recent contributions appeared during the COVID-19 pandemic, we also recall the recent papers [9, 5] where a meta-community SEIR-like model has been proposed and employed to reproduce the contagion in Italy.

Moreover, the highly heterogeneous quality of COVID-19 data requires the design of sophisticated model calibration procedures able to deal with the intrinsic ill-posedness of the inverse problem (the calibration) and going beyond, e.g., the popular approach based on a least square minimization approach which, typically, does not incorporate any quality information on data.

In view of the above discussion, in this paper we generalize the SIDARTHE model by adding suitable spatial-multicity mobility terms. The resulting model is first calibrated based on Italian data to reproduce the COVID-19 contagion in Italy. Moreover, the robustness of the calibration process is assessed with the aim of exploring the capability of the model in producing reasonable forecast.

The outline of the paper is as follows: in Section 2 we introduce the mathematical model, Section 3 is devoted to the description of the calibration procedure, Section 4 and Section5 contain the obtained numerical result along with a critical discussion.

2 Mathematical model

The spread of COVID-19 has been characterized by a very peculiar behaviour: in particular it has been emphasized by several authors that it is of paramount importance to consider a compartment describing the the dynamics of infected undetected individuals. For this reason in this paper the SIDARTHE model presented in [10] will represent our point of departure. The model is described

by the following system of ordinary differential equations

$$\begin{aligned}
\dot{S}(t) &= -S(t)\frac{\alpha I(t)+\beta D(t)+\gamma A(t)+\delta R(t)}{N},\\
\dot{I}(t) &= S(t)\frac{\alpha I(t)+\beta D(t)+\gamma A(t)+\delta R(t)}{N}-(\varepsilon+\zeta+\lambda)I(t),\\
\dot{D}(t) &= \varepsilon I(t)-(\eta+\rho)D(t),\\
\dot{A}(t) &= \zeta I(t)-(\theta+\mu+\kappa)A(t),\\
\dot{R}(t) &= \eta D(t)+\theta A(t)-(\nu+\xi)R(t),\\
\dot{T}(t) &= \mu A(t)+\nu R(t)-(\sigma+\tau)T(t),\\
\dot{H}(t) &= \lambda I(t)+\rho D(t)+\kappa A(t)+\xi R(t)+\sigma T(t),\\
\dot{E}(t) &= \tau T(t).
\end{aligned} \tag{1}$$

where the compartments of the model are defined as (see Figure 1):

- S: number of susceptible (uninfected) individuals;
- I: number of infected (asymptomatic infected, undetected) individuals;
- D: number of diagnosed (asymptomatic infected, detected) individuals;
- A: number of ailing (symptomatic infected, undetected) individuals;
- R: number of recognized (symptomatic infected, detected) individuals;
- T: number of threatened (acutely symptomatic infected, detected) individuals;
- H: number of healed (recovered) individuals;
- E: number of extinct individuals;

and $N = S + I + D + A + R + T + H + E$ denotes the total population (assumed constant).

The model is characterized by the following 16 parameters:

- α, β, γ and δ denote the transmission rates due to contacts between a susceptible subject and an infected, a diagnosed, an ailing or a recognized subject;
- ϵ and θ describe the probability rate of detection, relative to asymptomatic and symptomatic cases, respectively;
- ζ and η denote the probability rate at which an infected subject, respectively not aware and aware of being infected, develops clinically relevant symptoms;
- μ and ν respectively denote the rate at which undetected and detected infected subjects develop life-threatening symptoms;
- τ denotes the mortality rate;

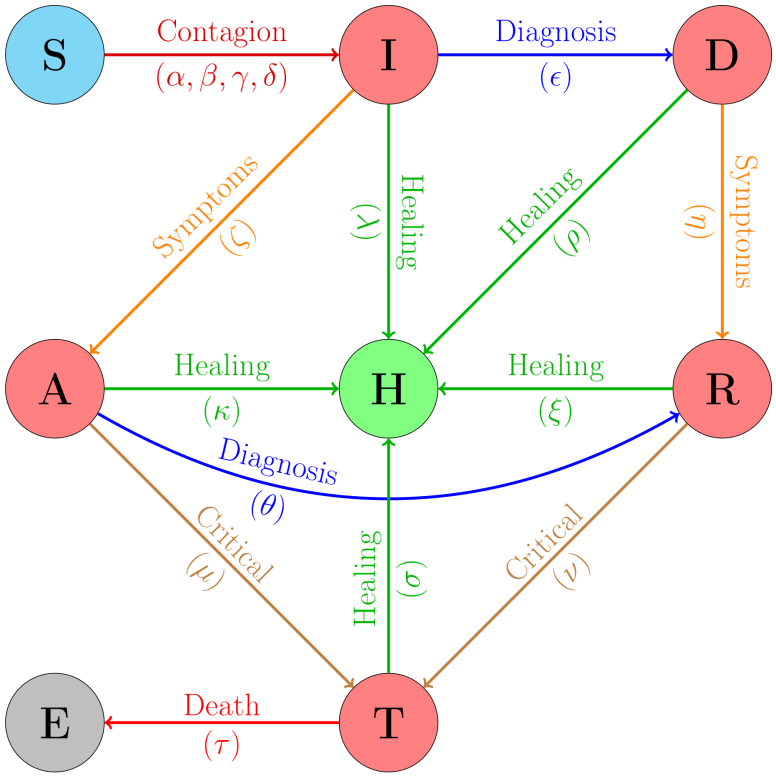

Figure 1: Interactions between compartments in SIDARTHE model.

- $\lambda, \rho, \kappa, \xi$ and σ denote the rate of recovery for the five classes of infected subjects.

For a more detailed description of the SIDARTHE model we refer to [10].

In mathematical epidemiology a fundamental quantity is the *basic reproduction number* (denoted by R_0) which is used to measure the transmission potential of a disease. It represents the average number of secondary infections produced by a typical case of an infection in a population where everyone is susceptible (see [6, 15]). In the SIDARTHE model we have

$$R_0 = \frac{\alpha + \beta\varepsilon/r_2 + \gamma\zeta/r_3 + \delta\left(\eta\varepsilon/\left(r_2 r_4\right) + \zeta\theta/\left(r_3 r_4\right)\right)}{r_1}, \tag{2}$$

where $r_1 = \epsilon + \zeta + \lambda, r_2 = \eta + \rho, r_3 = \theta + \mu + \kappa, r_4 = \nu + \xi$ and $r_5 = \sigma + \tau$.

From the mathematical point of view the reproduction number plays the role of a threshold value for the dynamics of the system and the disease. If $R_0 > 1$, the disease remains in the population; if $R_0 < 1$, the number of infected gradually declines to zero, and the disease disappears.

2.1 Multi-city model

In order to account for a spatial characterization of the evolution of the epidemic, we consider a complete graph describing a geographic network characterized by C_n nodes (representing the fundamental geographic entities we want to account for *e.g.* regions, provinces, cities, etc...) (see

for example [3, 15]). The population of each node i is denoted by N_i and every node a system like (1) is associated. Moreover we introduce a *mobility matrix* M where the element m_{ij} represents the mobility of individuals from node j to node i (matrix M is the transpose of the so-called *origin-destination* matrix). By means of the mobility matrix we can compute the total number of infected people arriving at node i as $\sum_j m_{ij}\frac{I_j}{N_j}$; hence the probability of infection from all nodes to node i is given by $\sum_j m_{ij}\frac{I_j}{N_j}\alpha$ and the fraction of susceptible people at node i which can be infected by people from all other locations is given by

$$\dot{I}_{mob} = \frac{\sum_j m_{ij}\frac{I_j}{N_j}\alpha}{N_i^{\text{tot}}}, \tag{3}$$

where $N_i^{\text{tot}} = N_i + \sum_j m_{ij}$ denotes the total number of individuals in location i including the mobility contribution.

We assume that the only infected compartment that contributes to spatial spreading is I (infected undetected) since it is reasonable to assume that the detected (D, R, and T) and the symptomatic (A) do not move. Based on these assumptions the spatial evolution of the disease is described by C_n systems of ODEs where each system is a modification of the SIDARTHE "single-city" model (1) that reads

$$\begin{aligned}
\dot{S}_i(t) &= -S_i(t)\frac{\alpha(I_i(t)+\sum_j \frac{m_{ij}}{N_j}I_j(t)) + \beta D_i(t) + \gamma A_i(t) + \delta R_i(t)}{N_i^{\text{tot}}},\\
\dot{I}_i(t) &= S_i(t)\frac{\alpha(I_i(t)+\sum_j \frac{m_{ij}}{N_j}I_j(t)) + \beta D_i(t) + \gamma A_i(t) + \delta R_i(t)}{N_i^{\text{tot}}} - (\varepsilon+\zeta+\lambda)I_i(t),\\
\dot{D}_i(t) &= \varepsilon I_i(t) - (\eta+\rho)D_i(t),\\
\dot{A}_i(t) &= \zeta I_i(t) - (\theta+\mu+\kappa)A_i(t),\\
\dot{R}_i(t) &= \eta D_i(t) + \theta A_i(t) - (\nu+\xi)R_i(t),\\
\dot{T}_i(t) &= \mu A_i(t) + \nu R_i(t) - (\sigma+\tau)T_i(t),\\
\dot{H}_i(t) &= \lambda I_i(t) + \rho D_i(t) + \kappa A_i(t) + \xi R_i(t) + \sigma T_i(t),\\
\dot{E}_i(t) &= \tau T_i(t),
\end{aligned} \tag{4}$$

In the results described in Section 4 we have used the origin-destination matrix available at the level of municipalities at `https://www.istat.it/it/archivio/139381`; these data have been collected in 2011 but the comparisons with some regional data available for 2019 show that minor changes have occurred during the last 8 years.

3 Parameter calibration

System (4) can be recast in the following general form describing a system of ODEs:

find $\mathbf{Y}(t) : [t_I, t_F] \to \mathbb{R}^{n_e}$ with $\mathbf{Y}(t) = [Y_1(t), \ldots, Y_{n_e}(t)]^T$ such that

$$\mathbf{Y}'(t) = \mathbf{F}(t, \mathbf{Y}(t); \mathbf{p}(t)) \quad t \in (t_I, t_F] \tag{5}$$

$$\mathbf{Y}(t_I) = \mathbf{Y}_0 \tag{6}$$

where the vector valued function $\mathbf{p}(t) : (t_I, t_F] \to \mathbb{R}^{n_p}$ encodes the (possibly time dependent) parameters of the problem.

Let us partition the interval $I = [t_I, t_F]$ into subintervals $I_j = [t_j, t_{j+1}]$, $j = 0, M-1$ with $t_0 = t_I$ and $t_M = t_F$.

Let us introduce the set of admissible parameters

$$\mathcal{U}_{ad} = \{\mathbf{p}(t) : \mathbf{p}|_{I_j} \in [\mathbb{P}^0(I_j)]^{n_p}, \mathbf{p}_{L,j} \leq \mathbf{p}(t) \leq \mathbf{p}_{U,j}, t \in I_j, j = 1, \ldots, M-1\} \tag{7}$$

where $\mathbf{p}_{L,j}, \mathbf{p}_{U,j}$ are given constant vectors.

Let us assume the following collection of data are given

$$\{\mathbf{Y}^*_{1,j}, \ldots, \mathbf{Y}^*_{n_j,j}\}_{j=1}^M.$$

The calibration process is performed by solving the following minimization problem

$$\mathbf{p}^*(t) = \text{argmin}_{\mathbf{p}\in\mathcal{U}_{ad}} \mathcal{J}(\mathbf{p}) + c\mathcal{R}(\mathbf{p}) \tag{8}$$

where

$$\mathcal{J}(\mathbf{p}) := \sum_{j=1}^{M} \sum_{i=1}^{n_j} \|\mathbf{Y}(t_i^{(j)}) - \mathbf{Y}^*_{i,j}\|^2 \tag{9}$$

being $\mathbf{Y}(t_i^{(j)})$ the solution of (5)-(6) evaluated at a certain given instant $t_i^{(j)} \in I_j$ and $\|\cdot\|$ the usual Euclidean vector norm. The regularization term $\mathcal{R}(\mathbf{p})$ is weighted by a penalization term $c > 0$.

The above procedure can be generalized in case the following collection of data are given

$$\{(Y_s)^*_{1,j}, \ldots, (Y_s)^*_{n_j,j}\}_{j=1}^M, \qquad s \in \{s_1, \ldots, s_d\}.$$

It is sufficient to consider

$$\mathcal{J}(\mathbf{p}) := \sum_{j=1}^{M} \sum_{i=1}^{n_j} \sum_{s\in\{s_1,\ldots,s_d\}} ((Y_s)(t_i^{(j)}) - (Y_s)^*_{i,j})^2. \tag{10}$$

For the calibration of the model, we employed the regularization term

$$\mathcal{R}(\mathbf{p}) = \sum_{j=1}^{M} \sum_{i=1}^{n_j} \|\mathbf{Y}''(t_i^{(j)})\|^2$$

where the values of the second derivatives are approximated with a centered difference formula. We considered the official epidemiological data supplied daily by the Dipartimento della Protezione Civile (DPC) through the repository `https://github.com/pcm-dpc/COVID-19`. The accuracy of this data is highly questioned, in particular concerning the estimate of the total number of infection (which is strongly dependent on the screening effort). Among the DPC data, we have selected 4 time series that can be considered more reliable and have a reasonable correspondence with the compartments of the SIDARTHE model: the infected individuals quarantined at home (corresponding to the Detected compartment D), the symptomatic hospitalized cases (corresponding to the Recognized compartment R), the cases in ICUs (corresponding to the Threatened compartment T) and the cumulative number of fatalities (corresponding to the Extinct compartment E).

The calibration has been performed solving the minimization problem (8) with $c = 1$, by a parallel version of the limited memory Broyden-Fletcher-Goldfarb-Shanno algorithm with box constraints (L-BFGS-B), see [17] for details.

4 Results

In this section we present the results that have been obtained using the model and the data introduced above in order to evaluate the forecasting capabilities of the model.

A first analysis was finalized to evaluate the dependence of the calibration of the model (4), based on the fitting strategy introduced in Section 3, on the number of days of recorded data used for the data calibration. This kind of analysis could be used to assess at which extent the model may be able to forecast the time evolution of the epidemic beyond the available recorded data.

We have considered 6 phases over the time in which the model parameters assume different values as a consequence of the political choices that led to progressive restrictions and changes in the case detection strategy. The first 5 phases correspond to those considered in [10]. While in [10] the model was started on February 20th, in the present work day 0 is February 25th, the first day for which spatial distributed data at the provincial level were made available in the DPC database.

Note that at day 0, some hygiene and behavioral recommendations were already issued, together with the first government restriction measures (school closure) inducing a certain degree of awareness of the epidemic in the population. The second phase starts at day 7 when the screening was limited to symptomatic individuals. On day 17, a first partial lockdown was introduced limiting the movement of people in the northern Italian regions. The national lockdown was enforced at day 23 while at day 33 a broader testing campaign allowed to identify a larger number of mildly symptomatic infected cases. In this work, we have considered an additional phase starting at day 68, corresponding to the partial relaxation of containment measures that was issued on May 3rd.

The multi-city SIDARTHE model (4) has been calibrated using a number of days of recorded data ranging between 40 and 110 starting from February 25th.

In Figure 2 we present a comparison between the time evolution computed by our model and the corresponding data at the national level. In particular, the different curves correspond to the compartments that have been used for the calibration, namely the diagnosed cases (D), the recognized cases (R), the threatened cases (T) and the extincts (E).

As already pointed out in [10], the calibration of this kind of models involving many state variables and a large number of uncertain parameters is a very challenging problem which is in general ill-posed. In this respect, many different parameter sets may all potentially match the recorder data with a similar degree of accuracy. However, the result of the parameter calibration, which is reported in Table 1, displays values of the parameters which are close to those obtained in [10] .

As mentioned above, the model has been calibrated using the compartments that have a correspondent counterpart in the recorded data.

An estimate of the total number of infected can be obtained summing all the infected compartments (I+D+A+R+T) including those (I and A) that, being undetected, cannot appear in the recorded data.

The time history of all the infected compartments is displayed in Figure 3. It should be pointed out that the cumulative count predicted by the model indicated that the total number of cases will be close to one million.

The calibration carried out in this work has been based on time history of number of individuals populating the different compartments at the national level. However, the extended multi-city model that we have considered allows to analyse the spatial spreading of the epidemic. Figure 4 shows the point prevalence at different times during the outbreak, that is the ratio between the total number of people infected at a given time in each province and the population living in that

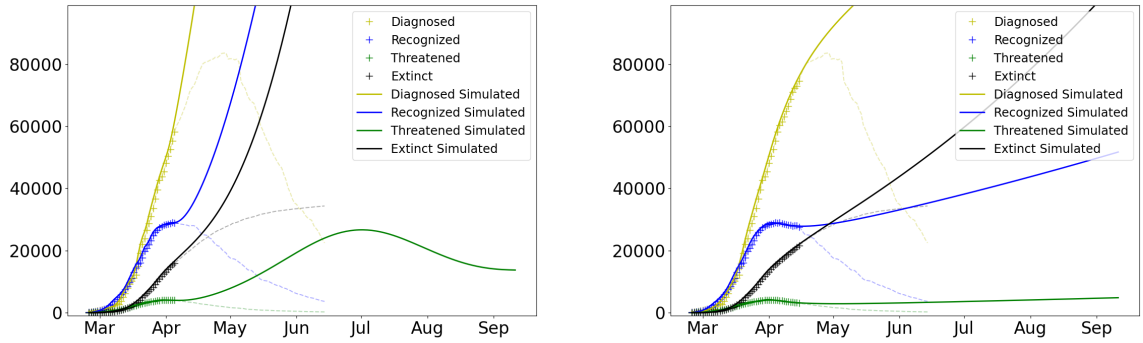

(a)

(b)

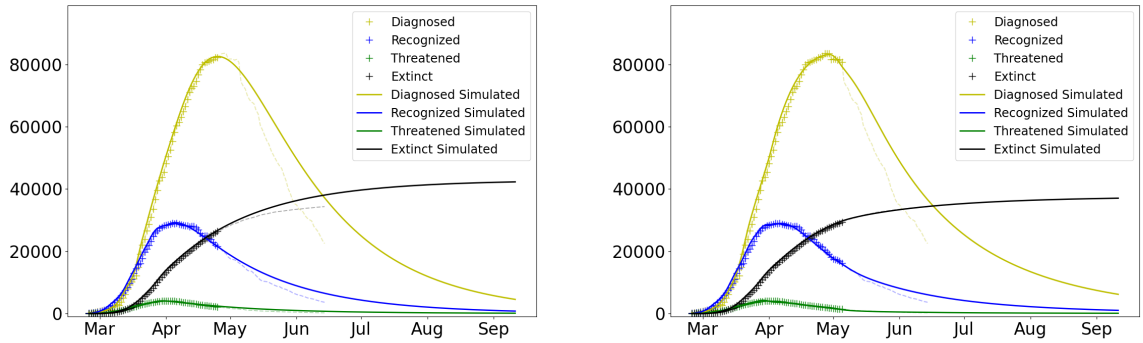

(c)

(d)

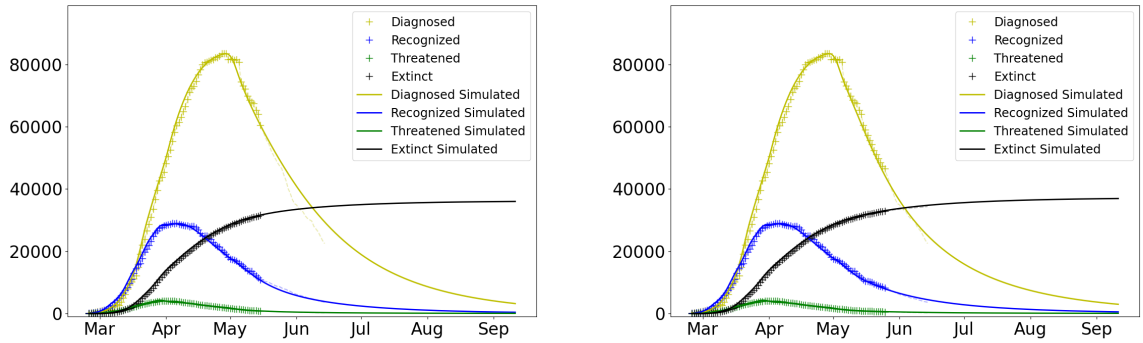

(e)

(f)

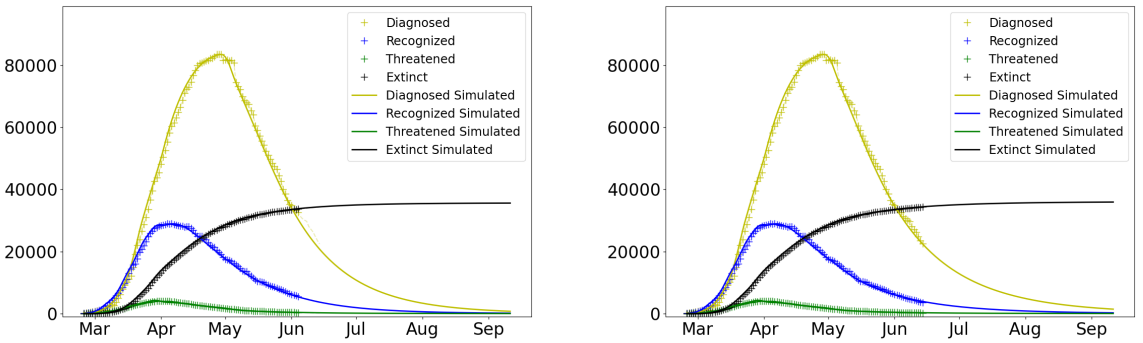

(g)

(h)

Figure 2: Comparison of the simulation results with the official data for the compartments that have been used for the model calibration with different training sets until day 40 (a), day 50 (b), day 60 (c), day 70 (d), day 80 (e), day 90 (f), day 100 (g), day 110 (h).

Table 1: Values of the model parameters during the different phases

	Phase 1	Phase 2	Phase 3	Phase 4	Phase 5	Phase 6
α	0.6238	0.4147	0.3998	0.3179	0.1900	0.2351
β	0.3181	0.0369	0.0164	0.0038	0.0010	0.0187
δ	0.0870	0.0378	0.0109	0.0034	0.0010	0.1395
γ	0.4694	0.3052	0.3027	0.2576	0.0449	0.3239
ϵ	0.2274	0.1264	0.1231	0.1470	0.0389	0.2751
θ	0.4179	0.3695	0.3770	0.3065	0.3893	0.1916
ζ	0.4262	0.2022	0.0851	0.0145	0.0594	0.0010
η	0.2502	0.0767	0.0314	0.0564	0.0010	0.0286
μ	0.0692	0.0387	0.0320	0.0011	0.0892	0.0093
ν	0.0442	0.0414	0.0445	0.0464	0.0010	0.0198
τ	0.0539	0.1821	0.2329	0.2059	0.1723	0.1929
λ	0.0072	0.0585	0.0590	0.1126	0.1203	0.0742
ρ	0.0042	0.0066	0.1205	0.2121	0.0154	0.1173
κ	0.0357	0.0081	0.0351	0.0010	0.0617	0.0013
ξ	0.0078	0.0836	0.0700	0.0543	0.1229	0.1805
σ	0.0042	0.0471	0.0417	0.0586	0.0761	0.1300

province.

A similar analysis has been carried out in order to evaluate what would have been the epidemic evolution in the absence of the strict national lockdown measures. In this case, neglecting the change of parameters after day 17, that is extending the Phase 3 in the future, the spatial spread of the epidemic predicted by the model is displayed in Figure 5 (where we have used the same scale as in 4).

5 Discussion

In the recorded data, the peak of the cases threatened in ICUs (April 3rd, day 38, 4068 cases) anticipates by one day the peak of the recognized cases (April 4th, day 39, 29010) which, in turns, occurs more than 3 weeks before the peak of the diagnosed cases (April 29th, day 64, 83652 cases).

The comparison displayed in Figure 2 clearly highlights that even a qualitative prediction of the evolution of the epidemic appears to be difficult until the data used in the calibration cover the three peaks.

Indeed, the calibration that uses 60 days of recorded data is the first one to be able to reproduce the decreasing trends of all the compartments, while the error between the simulated results with respected to the recorded data (not used for the model training) considerably reduces when at least two weeks of recorded data past the latest peak occurs, that is data until day 80, are used.

Notice that the prediction using recorder data until day 70 still overestimates the total number of hospitalized cases (R+T) at mid June by almost the 90%.

These results clearly indicates that a particular care should be paid when a model calibrated with a partial time history is used for forecasting, in particular when the level of uncertainty of the data is high.

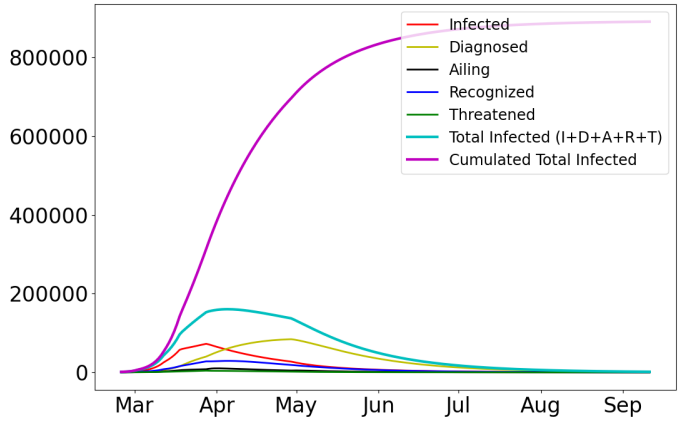

Figure 3: Time history of all the infected compartments and cumulative count of the total infected cases.

The epidemic spreading results presented in Figures 4 and 5 indicate that the considered model could represent a valid tool to investigate the spatial evolution of the disease. The level of accuracy of the spatial evolution may be further improved by considering in the calibration spatial dependent parameters and exploiting the spatial distribution of the recorded data (as done, for instance, in [5]).

The computational model here proposed is highly efficient: every spatio-temporal simulation at the provincial scale (107 geographical units) over a time range of 1 year requires less than 1 second on a laptop. The calibration procedure is computationally more involved. However, running the parallel L-BFGS-B model on a two-processor workstation with 24 cores the calibration can be obtained in a few minutes. This very low computational time allows real time considerations of multiple scenarios and is easily compatible with the implementation of an optimal control procedure aimed at identifying optimal strategies at both regional and local levels.

References

[1] Johns hopkins university. covid-19 dashboard by the center for systems science and engineering, last accessed june 23 2020. https://coronavirus. jhu.edu/map.html.

[2] L. J. S. Allen, B. M. Bolker, Y. Lou, and A. L. Nevai. Asymptotic profiles of the steady states for an *SIS* epidemic patch model. *SIAM J. Appl. Math.*, 67(5):1283–1309, 2007.

[3] Julien Arino and P. van den Driessche. A multi-city epidemic model. *Mathematical Population Studies*, 10(3):175–193, 2003.

[4] Duygu Balcan, Vittoria Colizza, Bruno Gonçalves, Hao Hu, José J. Ramasco, and Alessandro Vespignani. Multiscale mobility networks and the spatial spreading of infectious diseases. *Proceedings of the National Academy of Sciences*, 106(51):21484–21489, 2009.

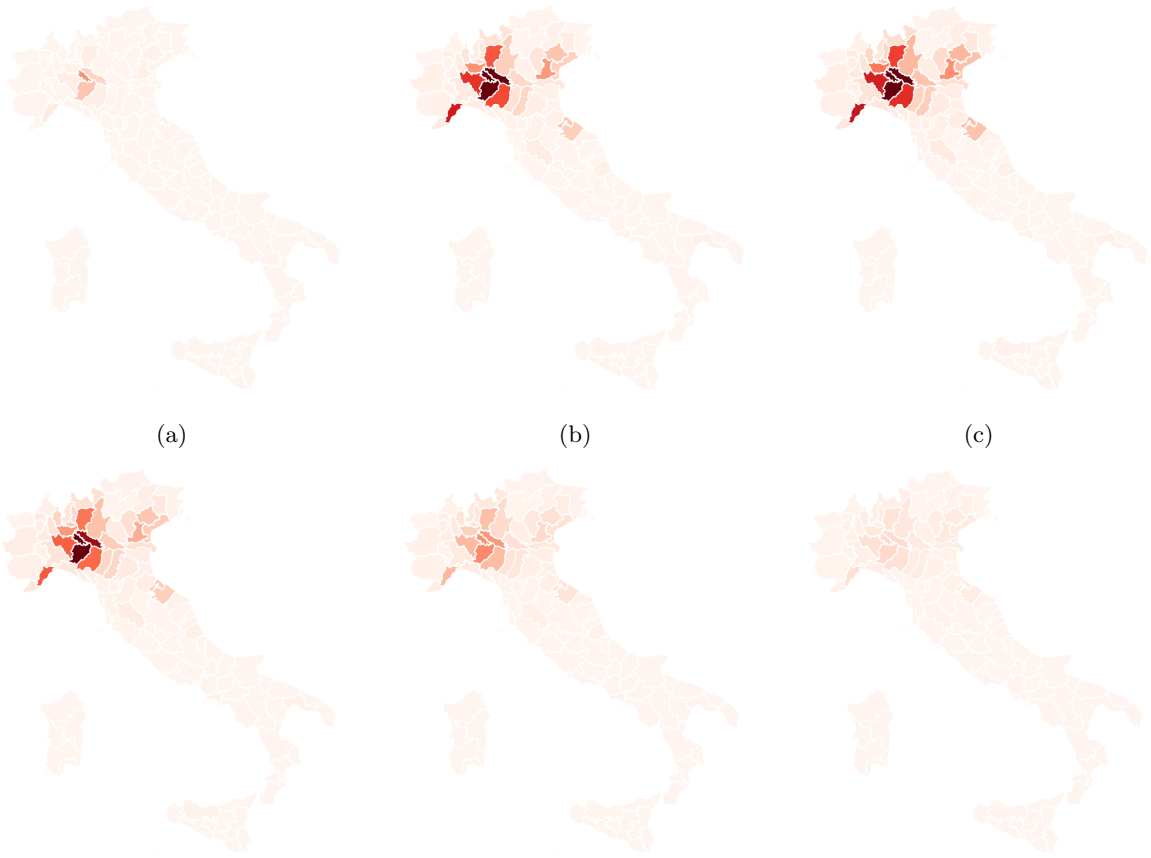

(a) (b) (c)

(d) (e) (f)

Figure 4: Point prevalence of the total infected (I+D+A+R+T compartments) predicted by the calibrated model at different times (a) Day 10, (b) Day 30, (c) Day 50, (d) Day 70, (e) Day 90, (f) Day 110.

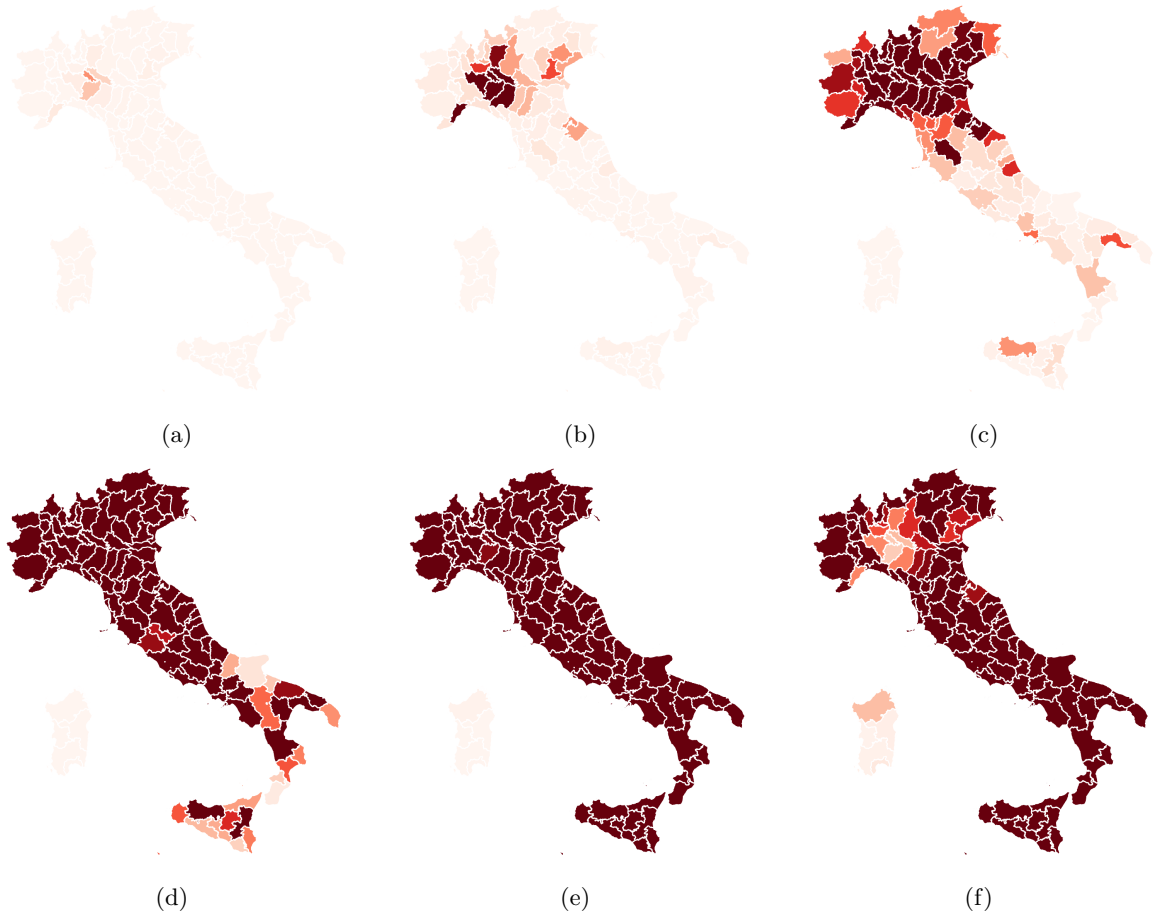

Figure 5: Point prevalence of the total infected (I+D+A+R+T compartments) predicted in the absence of the national lockdown (a) Day 10, (b) Day 30, (c) Day 50, (d) Day 70, (e) Day 90, (f) Day 110.

[5] Enrico Bertuzzo, Lorenzo Mari, Damiano Pasetto, Stefano Miccoli, Renato Casagrandi, Marino Gatto, and Andrea Rinaldo. The geography of covid-19 spread in italy and implications for the relaxation of confinement measures. *medRxiv*, 2020.

[6] Fred Brauer, Carlos Castillo-Chavez, and Zhilan Feng. *Mathematical models in epidemiology*. Springer, 2019.

[7] Dongmei Chen, Bernard Moulin, and Jianhong Wu. *Analyzing and modeling spatial and temporal dynamics of infectious diseases*. John Wiley & Sons, 2014.

[8] Vittoria Colizza, Alain Barrat, Marc Barthélemy, and Alessandro Vespignani. The role of the airline transportation network in the prediction and predictability of global epidemics. *Proceedings of the National Academy of Sciences*, 103(7):2015–2020, 2006.

[9] Marino Gatto, Enrico Bertuzzo, Lorenzo Mari, Stefano Miccoli, Luca Carraro, Renato Casagrandi, and Andrea Rinaldo. Spread and dynamics of the covid-19 epidemic in italy: Effects of emergency containment measures. *Proceedings of the National Academy of Sciences*, 117(19):10484–10491, 2020.

[10] Giulia Giordano, Franco Blanchini, Raffaele Bruno, Patrizio Colaneri, Alessandro Di Filippo, Angela Di Matteo, and Marta Colaneri. Modelling the covid-19 epidemic and implementation of population-wide interventions in italy. *Nature Medicine*, pages 1–6, 2020.

[11] Herbert W. Hethcote. The mathematics of infectious diseases. *SIAM Rev.*, 42(4):599–653, 2000.

[12] William Ogilvy Kermack and Anderson G McKendrick. A contribution to the mathematical theory of epidemics. *Proceedings of the royal society of london. Series A, Containing papers of a mathematical and physical character*, 115(772):700–721, 1927.

[13] Adam J Kucharski, Timothy W Russell, Charlie Diamond, Yang Liu, John Edmunds, Sebastian Funk, Rosalind M Eggo, Fiona Sun, Mark Jit, James D Munday, Nicholas Davies, Amy Gimma, Kevin [van Zandvoort], Hamish Gibbs, Joel Hellewell, Christopher I Jarvis, Sam Clifford, Billy J Quilty, Nikos I Bosse, Sam Abbott, Petra Klepac, and Stefan Flasche. Early dynamics of transmission and control of covid-19: a mathematical modelling study. *The Lancet Infectious Diseases*, 20(5):553 – 558, 2020.

[14] Benjamin F. Maier and Dirk Brockmann. Effective containment explains subexponential growth in recent confirmed covid-19 cases in china. *Science*, 368(6492):742–746, 2020.

[15] Maia Martcheva. *An introduction to mathematical epidemiology*, volume 61. Springer, 2015.

[16] Fei-Ying Yang, Wan-Tong Li, and Shigui Ruan. Dynamics of a nonlocal dispersal SIS epidemic model with Neumann boundary conditions. *J. Differential Equations*, 267(3):2011–2051, 2019.

[17] Ciyou Zhu, Richard H. Byrd, Peihuang Lu, and Jorge Nocedal. Algorithm 778: L-bfgs-b: Fortran subroutines for large-scale bound-constrained optimization. *ACM Trans. Math. Softw.*, 23(4):550–560, December 1997.

MOX Technical Reports, last issues

Dipartimento di Matematica
Politecnico di Milano, Via Bonardi 9 - 20133 Milano (Italy)

39/2020 Martinolli, M.; Biasetti, J.; Zonca, S.; Polverelli, L.; Vergara, C.
Extended Finite Element Method for Fluid-Structure Interaction in Wave Membrane Blood Pumps

40/2020 Fresca, S.; Manzoni, A.; Dedè, L.; Quarteroni, A.
Deep learning-based reduced order models in cardiac electrophysiology

41/2020 Cannistrà,M.; Masci, C.; Ieva, F.; Agasisti, T.; Paganoni, A.M.
Not the magic algorithm: modelling and early-predicting students dropout through machine learning and multilevel approach

38/2020 Sollini, M.; Kirienko, M.; Cavinato, L.; Ricci, F.; Biroli, M.; Ieva, F.; Calderoni, L.; Tabacchi,
Methodological framework for radiomics applications in Hodgkin's lymphoma

34/2020 Antonietti, P.F.; Mazzieri, I.; Nati Poltri, S.
A high-order discontinuous Galerkin method for the poro-elasto-acoustic problem on polygonal and polyhedral grids

35/2020 Morbiducci, U.; Mazzi, V.; Domanin, M.; De Nisco, G.; Vergara, C.; Steinman, D.A.; Gallo, D
Wall shear stress topological skeleton independently predicts long-term restenosis after carotid bifurcation endarterectomy

36/2020 Pellagatti, M.; Masci, C.; Ieva, F.; Paganoni A.M.
Generalized Mixed-Effects Random Forest: a flexible approach to predict university student dropout

37/2020 Fumagalli, A.; Scotti, A.
A mathematical model for thermal single-phase flow and reactive transport in fractured porous media

31/2020 Bernardi, M.S.; Africa, P.C.; de Falco, C.; Formaggia, L.; Menafoglio, A.; Vantini, S.
On the Use of Interfeometric Synthetic Aperture Radar Data for Monitoring and Forecasting Natural Hazards

32/2020 Menafoglio, A.; Sgobba, S.; Lanzano, G.; Pacor, F.
Simulation of seismic ground motion fields via object-oriented spatial statistics: a case study in Northern Italy